Supporting Information

Single glucose molecule transport process revealed by force tracing and molecular dynamics simulations

1. Force tracing experiments

1.1 The force tracing setup and response time details.

A laser beam is reflected by the AFM cantilever (Figure S1). The photodetector monitors the laser position and records the AFM cantilever displacement. We engaged the AFM tip using the commercial Picoscan software, and acquired force-distance curves on the living cell to locate the contact point between the AFM tip and the cell surface[1]. The AFM tip was slowly moved to the contact point between the AFM tip and the cell surface through the feedback system; then, we turned off the feedback system. It was clearly shown that the deflection of the cantilever kept constant during approaching[2, 3], which suggests that there is no contact force from the cell surface. Additionally, the fluctuation of a living cell was measured by approaching a clean AFM tip to the cell surface and gently touching the cell membrane with a force of about 20 pN. We found that the fluctuation of the living cell membrane is very tiny[2, 3]. These results indicate that approaching the cantilever to the contact point and staying at the contact point can avoid felling any force from the cell surface. Figure 1B is the schematic showing the relation position between the tip and cell membrane. It has been reported that the PEG linker with a molecular weight of 2KD occupies spheres with diameters of around 4 nm[4]. This is consistent with other reports, in which they reported that the height of PEG linker modified on the surface is ~3 nm[5]. Hence, there is a soft layer of PEG molecules with a height of 3-4 nm between the tip apex and the cell surface after engaging tip to the contact point. During the transporting process, PEG linker was stretched and hence there is space for the cantilever to bend downward (Figure 1B). We also performed the force tracing measurements by retracting the tip 1

& 2 nm. By retracting the tip 1 or 2 nm, we got force distributions with the average force value of ~ 35 pN (Fig. S1B and C), which is similar to the force value we showed in the main text. All the results presented above suggest that approaching the tip to the contact point is suitable for recording the transporting process.

The vertical position of the cantilever was recorded using a PCI-DAQ board controlled using LabVIEW software, which can successfully monitor fast processes down to 1 μs. The response time (τ) of the cantilever we used was determined based on the equation: $\tau_c = Q/(\pi \times f_0)$[6], where Q ~ 1.6 is the Q- (quality-) factor and f_0 = 3.2 kHz is the resonance frequency of our cantilevers in liquid. Then the response time (τ) of the cantilever is calculated as ~16 μs (Figure S2).

To further confirm the force signal of transporting event obtained by Force Tracing, we test the sensitivity of the system by recording the deflection of AFM cantilever during the process of approaching the AFM tip in the working medium. Firstly, we kept the AFM tip in the working medium for several minutes to stabilize the system; subsequently, we approached the tip by 100 nm abruptly. As shown in Figure S3, the system was sensitive enough to detect the abrupt activity of the AFM tip. With the sampling rate of 20,000 Hz (the maximum sampling rate could be up to 1 MHz), the system of Force Tracing can acquire 20 samples per millisecond, which provides the capability to monitor the activity of single molecule transporting.

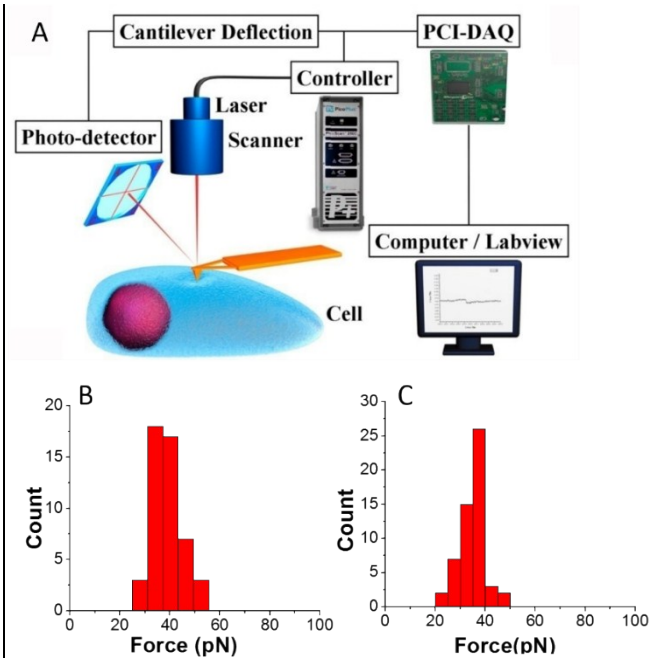

Figure S1. (A) Schematic setup of force tracing technique. (B) and (C) show the distribution of the glucose transport force for retracting the tip 1nm and 2 nm, respectively.

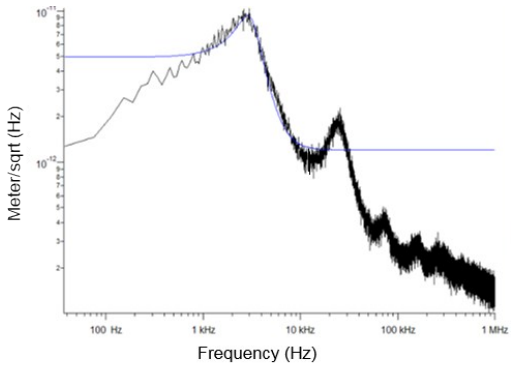

Figure S2. Thermal fluctuations of the cantilever.

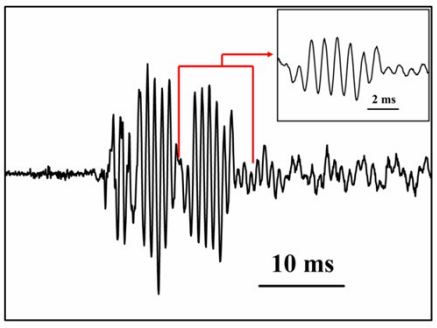

Figure S3. Tracing the sudden activity of AFM tip in the work medium. The deflection signals of AFM cantilever were clearly observed. The inset figure shows the magnification of the region as indicated by a red arrow.

The glucose molecules were attached to the AFM tip and allowed the molecule on tip apex to gently touch cell membranes. Once the glucose molecule was transported by GLUT1, the force signal from the sudden bending of AFM cantilever was recorded, showing the event of transporting a molecule into the cell. The force tracing technique has been demonstrated to be a powerful tool for studying the dynamics of substance transport via cell membranes at the single-molecule/particle level[2].

1.2 Determining the GLUT1 density and cellular glucose uptake for MDCK and HeLa cells

To confirm that there are more GLUT1s on the Hela cell membranes, we utilized semi-quantitative analysis of super resolution imaging (STORM) to estimate the number of GLUT1 per μm^2 of the cell membrane (Fig. S4). Meanwhile we measured the glucose uptake activity (Fig. S5). Both the results indicate that the GLUT1 number on HeLa cell membranes is much higher than that on MDCK cell membranes.

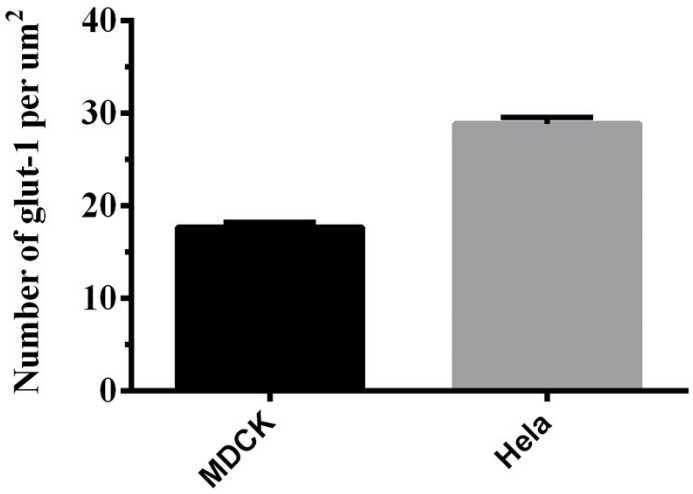

Figure S4. The semi-quantitative analyses of GLUT1 number on MDCK and Hela cell membranes by STORM. The unit is the GLUT1 number per μm^2. Date was from three independent experiments on cellular apical membranes, which were calculated via dividing the number of localizations per μm^2 by the average number of localizations from a single GLUT1.

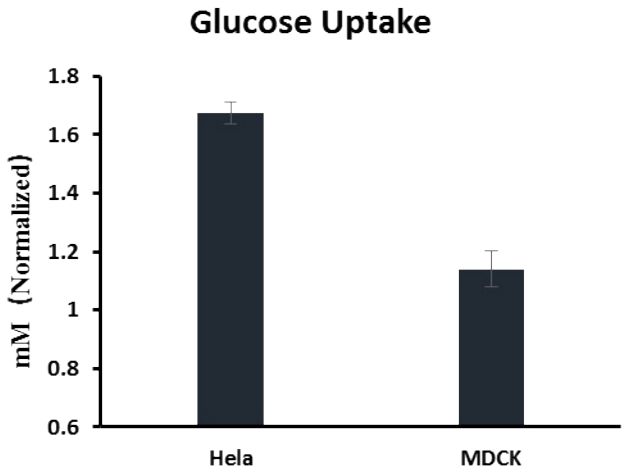

Figure S5. Glucose uptake in Hela and MDCK cells. Hela cells were cultured for glucose uptake assay and normalized to the level of MDCK cells.

1.3 The complete transporting event with PEG2000 is verified by using different length of linker.

We found that almost no force signal was detected while the linker (PEG690) with full extension of 3 nm was used. Fig. S6A shows a few events detected while using the PEG690, and the force values were smaller than the transporting force we detected. The force detected by using the linker (PEG1400) with contour length of 11 nm is 41± 10 pN (Fig.S6B), which similar to the force detected by using PEG2000 (Contour length ~20 nm). These results indicate that the linker with length of 11 nm (PEG1400) and 20 nm (PEG2000) is appropriate for studying membrane transport activity.

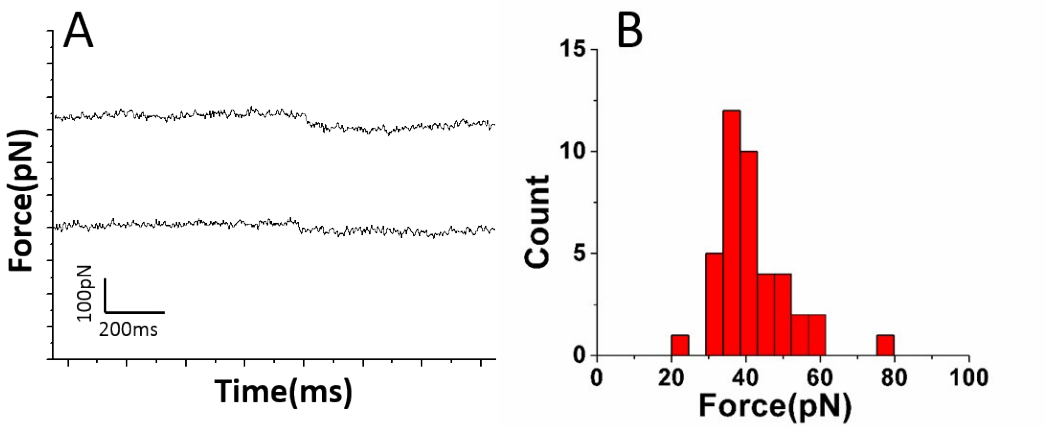

Figure S6. (A) Examples of the force tracing curves for the experiments using PEG690. (B) Distribution of the glucose transport force by using PEG1400 linker.

1.4 Locating the AFM tip on the monolayer of living cells.

To perform force measurements on the apical surface of the cells, we prepared a dense monolayer of HeLa cells on a glass slide surface. The AFM tip was positioned on top of the HeLa cell monolayer monitored by a CCD camera before the force tracing measurements (Figure S7). After one-hour incubation in glucose-free 1640 medium, the cells with diameter of 20-40 μm remained in close contact with each other, and the filopodia were normally extended, which indicated that the cells grew healthily on the glass slide surface.

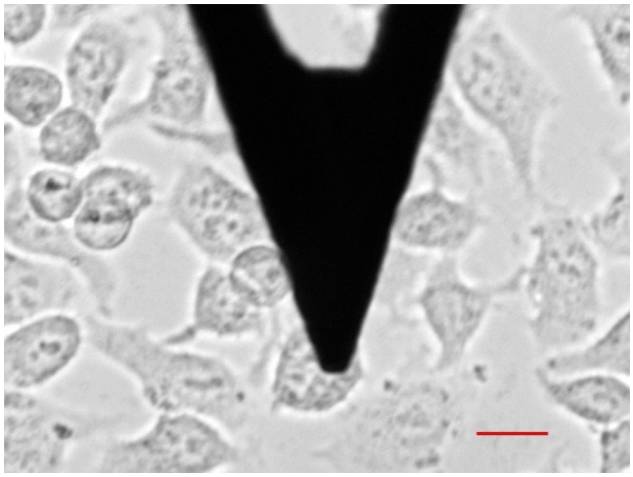

Figure S7. The optical image of AFM cantilever located above the living HeLa cell monolayer before performing Force Tracing test. The scale bar is 10 μm.

1.5 The regular force curve measurement by a glucose tethered AFM tip

We did regular force distance measurement to confirm that the PEG-glucose can be transported into the cell via GLUT1. A real typical force curve of D-glucose flowing into and pulled out of the cell membranes through GLUT1 is shown in Figure S8. The force curve started from right side, where the tip moved towards the cell surface. As the D-glucose on the tip touched on the cell surface, the slow slope appeared due to the contact between the cell and AFM tip. The slow slope of the force curve in Fig. S7 is the feature when engaging the force curve on living cells, because the cell is soft so that the cell may change the shape during the tip pressing on it. The force signal is based on the detection of small shifts of the cantilever-deflection signal that occur when D-

glucose on the AFM tip binds and unbinds to cell due to the interaction between D-glucose and the cell. The arrow head "fi" indicates that D-glucose on the tip was suddenly caught and transported into the cell by the glucose transporter as AFM tip approached to the cell surface (transporting force signal or catching D-glucose force signal). The arrow head "fu" indicates that the D-glucose was pulled out of the transporter as AFM tip withdrew from the cell (unbinding force signal). The unbinding event without transporting a molecule via the membrane only provides one "fu" peak in the force distance curve [7].

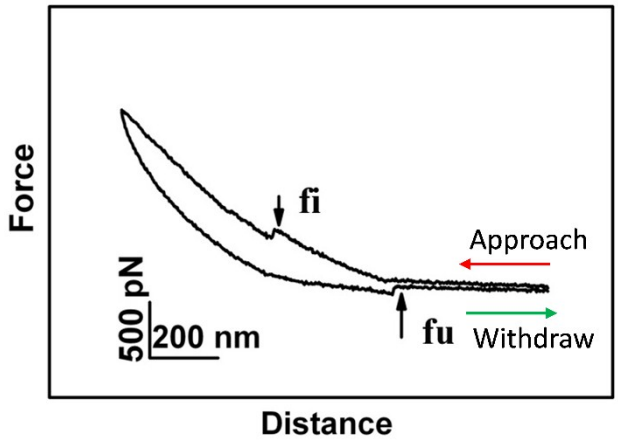

Figure S8. A curve of typical force-distance cycle obtained by a D-glucose-attached AFM tip on the starved living HeLa cell in a glucose-free medium. The cycle of force curve begins from right side. The arrow head "fi" indicates the force signal of transporting D-glucose on AFM tip into cell through glucose transporter in the cell membranes. The arrow head "fu" indicates the force signal of pulling D-glucose out of cell via the glucose transporter.

1.6 The measurement of a single glucose transportation distance

The stretching length x of PEG can be most appropriately calculated by the extended worm-like chain (WLC) model that characterizes the force (F)-dependent stretching behavior by the equation:

$$\frac{FL_p}{k_BT} = \frac{1}{4}\left(1 - \frac{x}{L_0} + \frac{F}{K_0}\right)^{-2} - \frac{1}{4} + \frac{x}{L_0} - \frac{F}{K_0} \quad (2)$$

Where k_B is the Boltzmann constant, T is the absolute temperature, L_p is the persistence length, K_0 is the enthalpic correction, and L_0 is the contour length. The persistence length is 3.8 ± 0.02 Å, and the enthalpic correction is 1561 ± 33 pN, as reported[8]. The contour length of PEG2000 (L_0) is estimated as 20 nm.

As the mean value of *F* 40 pN, the extension of the PEG2000 and PEG1400 linker is ~15 nm and ~7 nm, respectively. When using the PEG2000, the extension of the linker is more than the height of the GLUT1 receptors. This is because PEG2000 is long and flexible linker behaving as a random coil. Considering the AFM tip with the tip radius of ~20 nm, the molecules modified on the tip apex or on the side of the tip are detectable while performing force tracing experiments. In addition, assuming a random coil configuration for PEG, it estimates that the PEG linker with a molecular weight of 2KD occupies spheres with diameters of around 4 nm[4]. Considering diameters of PEG linker and the distance between modification position and tip apex, the actual movement distance of glucose is less than the theoretical extension of the linker calculated based on the force we detected.

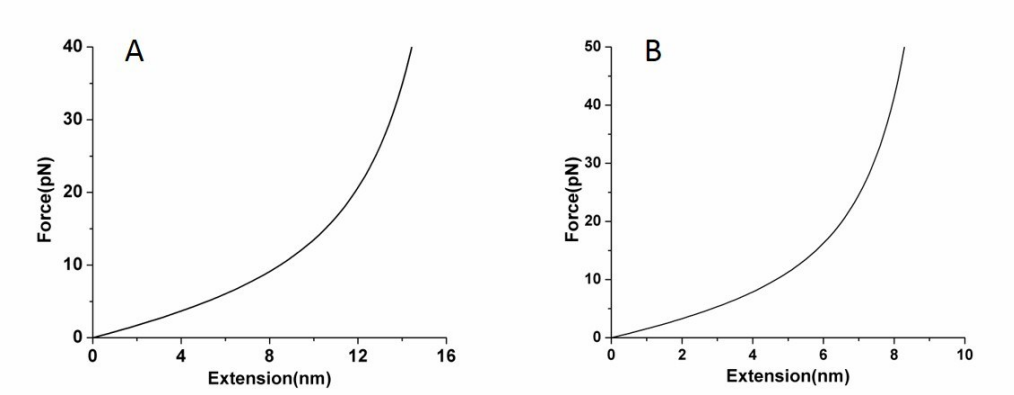

Figure S9. (A) The extension of PEG2000 linker according to the force. (B) The extension of PEG1400 linker according to the force.

2. Molecular dynamic (MD) simulations:

2.1 MD simulation set-up

The initial MD simulation system was built with CHARMM-GUI[9-11]web server using the CHARMM36 force field[12, 13]. The inward-open conformation of glucose transporter 1 (GLUT1) without the ligand β-D-glucopyranoside (β-NG) was obtained from the RCSB Protein Data Bank (pdb_id: 4PYP[14]). A DOPC bilayer with 300 molecules was used to merge the protein, and then the system was solvated with 23,758 TIP3P water molecules[15]. NaCl (0.1 M) was used to neutralize the system, resulting in

a total of approximately 120,000 atoms with initial dimensions 100 Å x 100 Å x 100 Å. The D-glucose ligand molecule was placed in the bulk solvent at a z distance of 10 Å above the bilayer.

The system was then equilibrated using Gromacs 5.0.4[16] based on the standard Membrane Builder protocol of CHARMM-GUI. Briefly, a Nosé–Hoover[17, 18]temperature-coupling method with a tau-t of 1ps was used to maintain a constant temperature of 303.15 K. A semi-isotropic Parrinello–Rahman[19, 20] method with a tau-p of 5 ps and a compressibility of 4.5×10^{-5}bar^{-1} was used for pressure coupling under NPT ensemble. The van der Waals interactions were smoothly switched off at 10−12Å by a force-switching function. Long-range electrostatic interactions were calculated using the particle-mesh-Ewald[21] method. All bond lengths involving hydrogen atoms were fixed using the LINCS[22] algorithm, enabling the 2-fs time step.

2.2 Steered molecular dynamics simulations

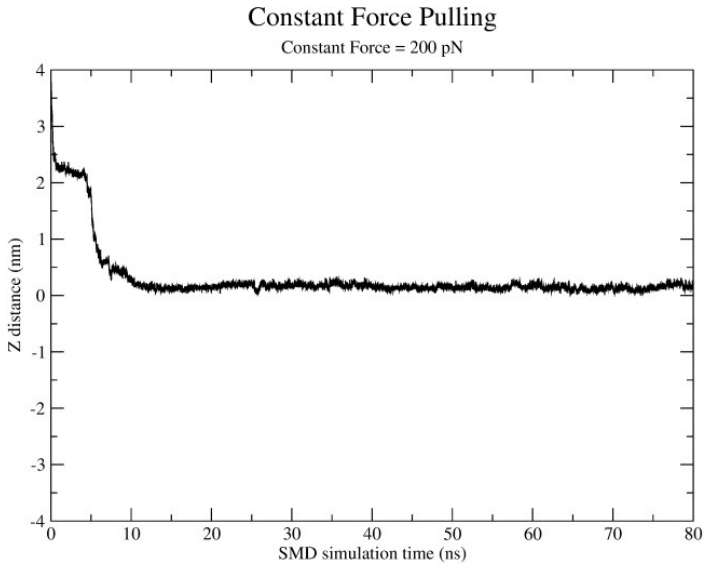

Figure S10. Constant force pulling SMD simulation.

We initiated our steered MD (SMD) simulation from the outward-open conformation of GLUT1 and exerted a large constant force of 200 pN on the centre of mass (COM) of D-glucose. As shown in Fig.S10, within our 80 ns constant force SMD simulation, neither the transport event of D-glucose nor the conformational transition of GLUT1 was observed. The D-glucose was trapped in the inner region of GLUT1, and a large

amount of simulation time was consumed in this site.

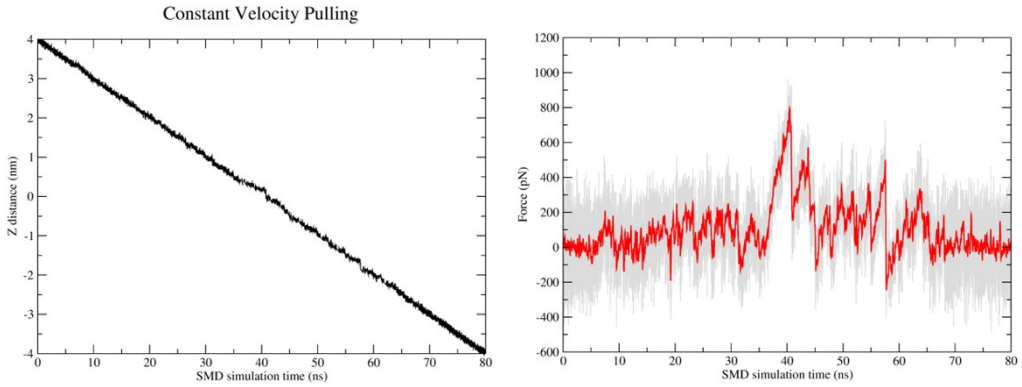

Figure S11. Constant velocity pulling SMD simulation with pulling speed of 1 Å/ns and the force profile experienced by D-glucose.

We also performed another set of constant-velocity SMD simulations using a speed as slow as 1 Å/ns (Fig. S11). However, the force experienced by the D-glucose during the constant-velocity SMD simulation was extremely large (approximately 800 pN at z= 0nm, corresponding to the position of the inner region of GLUT1.

2.3 Metadynamics simulation

Two collective variables (CVs) were biased here to explore the minimum free energy pathway (MFEP) of D-glucose transport through the GLUT1 channel and to broaden the conformational space of the transport process and structural transition. CV1 is defined as the conformational transition of GLUT1 from the outward-open state to the inward-open state. However, simulating the large-scale conformational change of a membrane protein is a challenging task. Fortunately, Branduardi *et al*[23] have provided an analytic expression to discern a reaction path to a sequence of intermediate conformations that can also be utilized as a CV in a path-metadynamics simulation. CV2 is defined as the distance between the COM of the D-glucose molecule and GLUT1to the z-axis.

To identify the outward-open state of GLUT1, we used the MODELLER[24] package to construct the outward-open conformation of GLUT1 using the bacterial homologue XylE[25] (PDB ID:4gby) as a template. Then, the adiabatic-bias molecular dynamics (ABMD) simulation[26], which exerts a ratchet-and-pawl-like restraint on the CV space,

was utilized to propel the conformation from the inward-open state (pdb 4PYP) to the outward-open state (our homology model). In this case, the Cα atoms of the transmembrane helical segments of GLUT1 were selected as CVs. Unlike SMD simulations, an ABMD simulation applies a harmonic potential that is zero when the conformation is moving towards the provided reference state and does not exert work on the system, thereby avoiding unphysical intermediate conformations during the transition. After a short ABMD simulation (5ns), the conformational transition was achieved, and a principal component analysis (PCA) was utilized to project the ABMD trajectory onto the first eigenvector. The corresponding conformations of the minimum and maximum eigenvalues along the first eigenvector exactly represented the fully outward-open and inward-open conformations of GLUT1 and 20 intermediate conformations that were generated as a path CV by interpolating the two states in the path-metadynamics simulation.

A two-dimensional well-tempered metadynamics simulation was implemented using Gromacs 5.0.4[16] and PLUMED[27] free energy calculation plugin. In the path CV along the conformational transition, two parameters were used to describe the position of the current state on the path (the s component indicated the position on the path; the z component indicated the position from the path). In this simulation, only s components were used as the CV1 to drive the conformational transition along the path. The height of the Gaussian hills was set to 0.5 kcal/mol, and the widths of the Gaussian hills were set to 0.1 for CV1 and 0.5 for CV2 with a pace step of 2000. A bias factor of 20 was used in the well-tempered metadynamics[28].

2.4 Recovering equilibrium properties initiated from metadynamics

Although metadynamics is a powerful sampling technique to explore rare events along the MFEP, obtaining converged free energy surface (FES) values for complex systems in a single run requires very long simulation times. In this case, we used an alternative method for conformational sampling by initializing massive short unbiased MD simulations from a metadynamics-sampled conformational space. It has been demonstrated by Huang et al.[29] that equilibrium thermodynamic properties can be

rapidly recovered from nonequilibrium simulation seeds.

Specifically, in this work, we first projected the metadynamics trajectories onto a 2D map defined by CV1 and CV2 (Fig. S12). Then, the map was divided into 0.2x0.2 grids, and the corresponding conformations in each grid were selected as the initial seeds to perform short, unbiased MD simulations using the OpenMM[30] package in GPU units. Note that in the first round of seed selection, not all the grids in a selected region were occupied by the metadynamics dataset. Then, we projected the set of unbiased MD trajectories onto the 2D map again to select the corresponding conformations in the empty grids, which were not recorded in the metadynamics simulation but were observed in the first round of unbiased MD runs to ensure that each grid had at least one seed in the selected region (approximately 1000 grids). Overall, 18μs (1800 seeds x 10ns) of unbiased MD simulations were conducted, and the final FES was estimated to be F= −logP/kT, where P is the stationary probability along the order parameter of our interest. The standard errors (less than 0.3 kT) were estimated from 1000 rounds of bootstrap resampling of the unbiased trajectories.

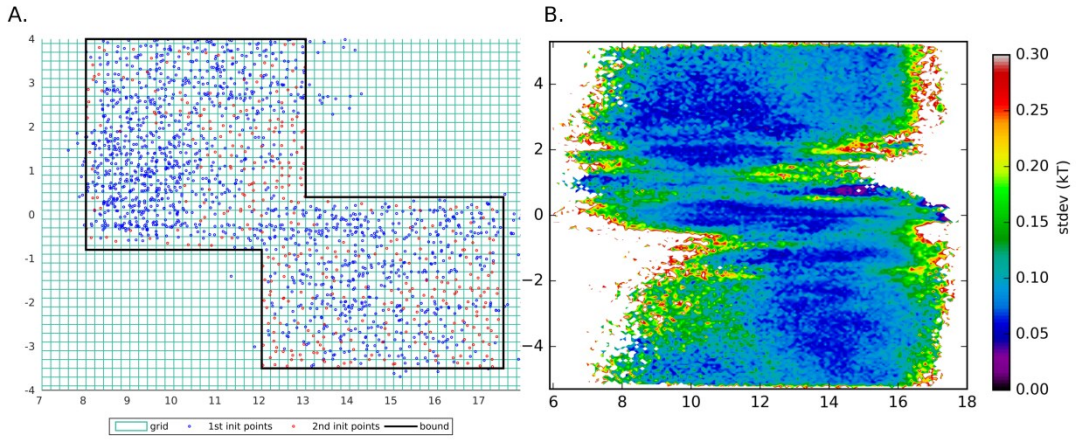

Figure S12(A) blue points indicate the selected seeds from metadynamic simulations by mapping the conformations onto CV1 and CV2 space and the red points indicate the selected seeds from the first rounded unbiased MD simulation trajectories. (B) The standard deviations of the free energy surface onto CV1 and CV2 space estimated from 1000 rounds of bootstrap resampling of the unbiased trajectories.

2.5 β-NG transporting simulations and mean force profile.

To mimic the transport process of PEG-conjugated D-glucose, a comparison MD simulation system was also built using 9-nonyl-β-D-glucopyranoside (β-NG) as the

ligand, which was co-crystallized in the inward-open conformation of GLUT1 (pdb:4PYP). The Swiss Param server was employed to generate the all-atom parameters of β-NG. A simulation protocol similar to that used in the D-glucose MD simulations was used. To calculate the FES of β-NG transport, a total of 15μs (1500 seeds x 10 ns) of unbiased MD simulation trajectories were generated to recover the equilibrium distributions. The 1D potential of mean force (PMF) along the z-axis was used to calculate the mean force profile (Fig.S13).

D-Glucose, connected via the hydrogen-bond interactions between the C4 and C6 hydroxyl (OH) groups of glucose and the carboxyl group of E41, flips 90° (from the conformation of glucose coloured with green to that coloured cyan) to enter the diffusion channel (Fig. S14).

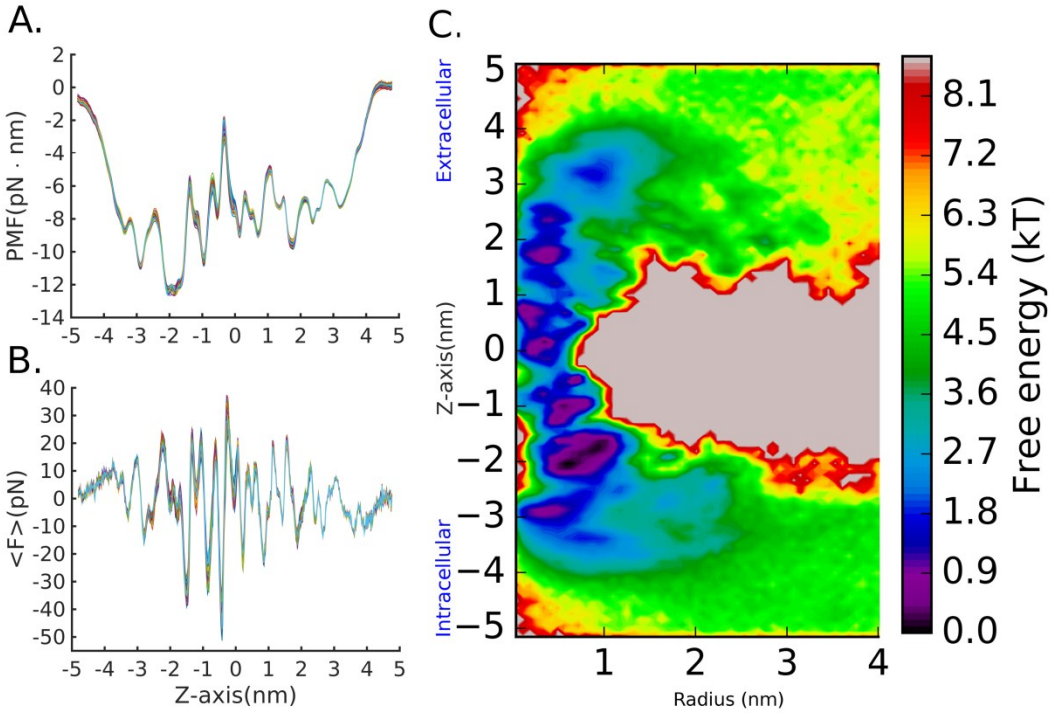

Figure S13. (A) One dimensional PMF of β-NG transporting along z-axis, and (B) the corresponding force profiles. 1000 rounds of bootstrap resampling of the unbiased trajectories were used to obtain the profiles. (C) 2D PMF of β-NG transporting by projecting the center of mass (COM) of the D-glucopyranoside group and GLUT1 onto the z-axis and xy-plane.

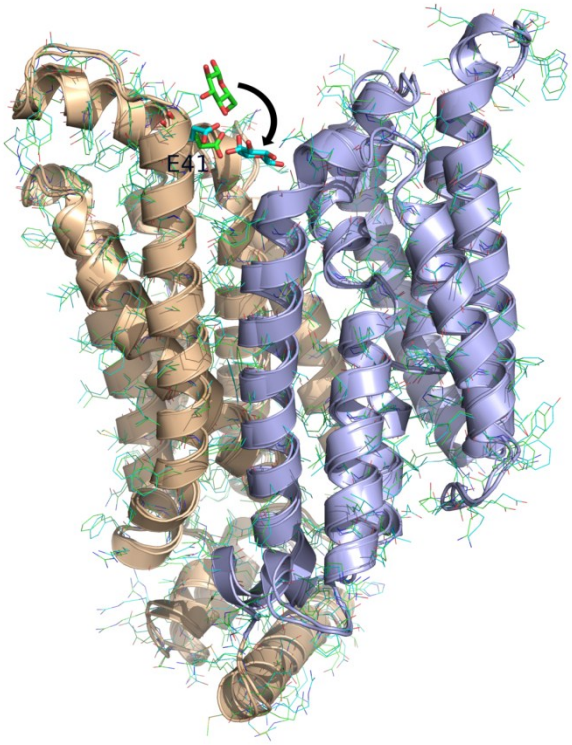

Figure S14. The key step of glucose entering the diffusion channel.

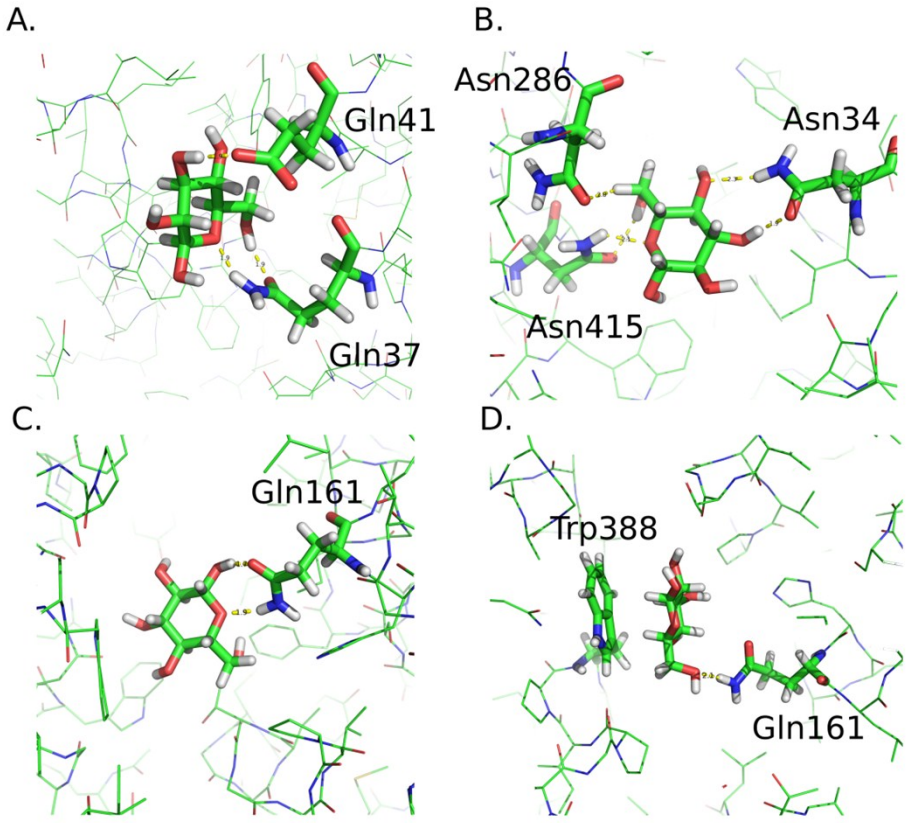

Figure S15. Key hydrogen-bonds regulating the glucose diffusion at various binding sites along the channel.

As shown in Fig. S15, hydrogen bonds formed (A) between the ring oxygen of glucose and the δ-amide group of Gln37, between the C6 OH group and the side chain δ-carboxyl oxygen of Gln37, and between the C3 OH group and the carboxyl group of Glu41, and (B) between the ring oxygen atom of glucose and the δ-amide group of Asn415; Asn34 can simultaneously act as both the hydrogen-bond donor (δ-amide group) and acceptor (δ-carboxyl oxygen) to contact the C4 and C3 OH groups of glucose. (C) The conserved Gln161 guides glucose diffusion. (D) The indole ring of Trp388 provides the π-π stacking interaction with the glucose ring to adjust the orientation of the glucose molecule to facilitate diffusion. The glucose located at various binding sites along the channel are shown in sticks, as well as the key residues providing the interactions.

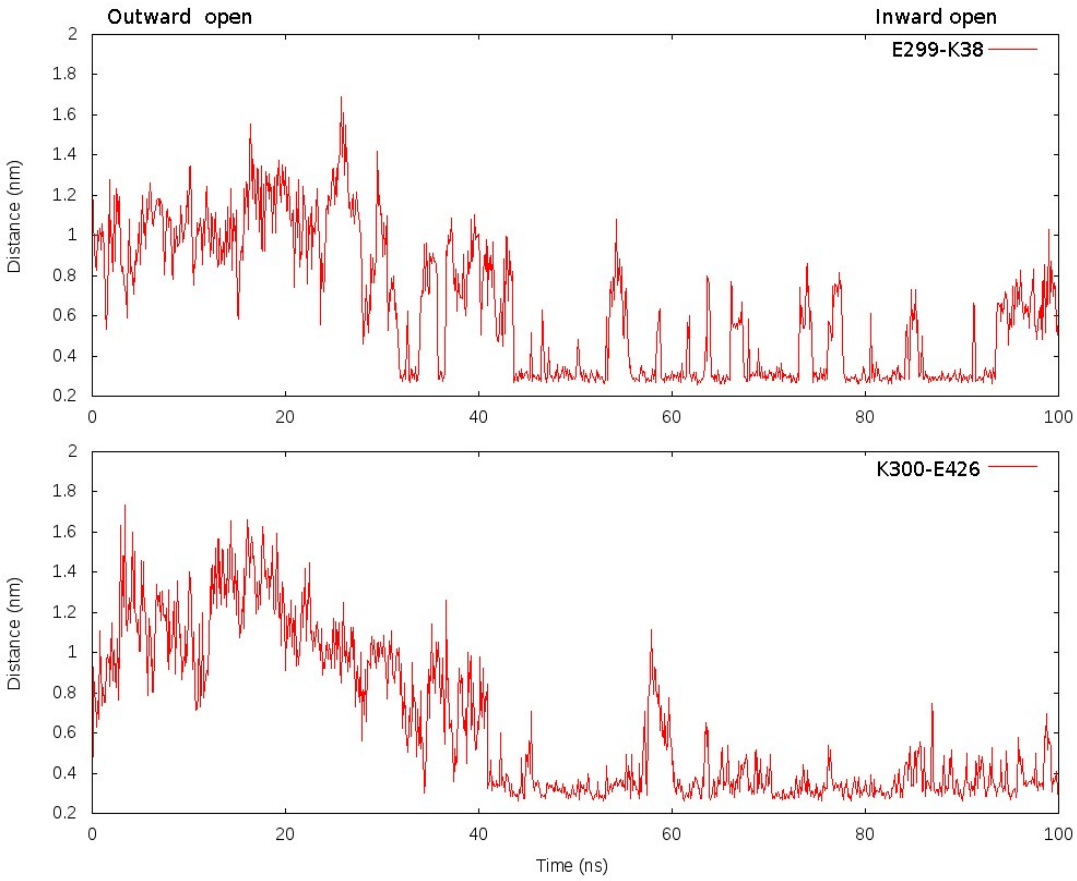

Figure S16. Salt bridge distances between E299/K38 and K300/E426 during our 100ns metadynamics simulation.

We began our simulation from the fully outward-open state of GLUT1; therefore, in the beginning of the simulation, the distance between these residues was as large as 0.9 nm, indicating that no salt bridge formed between these residues. As the bias accumulated in the metadynamics, the conformational transition occurred at 40 ns. Next, the two salt bridges were formed to stabilize the inward conformation. Moreover, the salt bridge between K300/E426 is more stable than that between E299/K38 (Fig. S15). This result is consistent with our mutation study in which the K300A mutant exhibited stronger glucose uptake inhibition.

2.6 Rate constants and the Arrhenius equation

The Arrhenius equation describes that the rate constant could be mathematically obtained by

$$k = A \cdot exp(-\frac{E_A}{RT})$$

Where E_A is activation energy, T is temperature, R is the gas constant, A is the pre-exponential factor. By taking the logarithm form of the equation, we obtain

$$lnk = lnA - \frac{E_A}{RT}$$

By assuming the pre-exponential factor A is constant, we can calculate the rate constant ratio between D-glucose and β-NG transporting using

$$ratio = \frac{k_{D-glucose}}{k_{\beta-NG}} = exp(-\frac{\Delta E_A}{RT})$$

Where ΔE_A is the activation free energy difference between D-glucose and β-NG transporting from our 1D-PMFs. Here, $\Delta E_A = 3.5564 \frac{kJ}{mol}$, $T = 303.15\ K$, $R = 8.314\ J/mol$. Then we estimated that the rate constant for D-glucose transporting is 4.1 fold faster than that of β-NG.

2.7 Standard free energy of binding from the potential of mean force

The pyEMMA[31] package was employed to analyze the unbiased MD simulation trajectories. To calculate the binding affinity of GLUT1 for D-Glucose, the massive short MD simulation trajectories were first mapped onto CV2 and CV3 space. Then the raw data was assigned into 1000 microstates using k-means clustering method with convergence tolerance of 1e-08. The Perron-cluster cluster analysis (PCCA) method[32] was used to compute the microstates into six metastable states (Fig.S16). Then binding free energy was computed by comparing the probabilities of the bound metastable states and its unbound metastable states[31, 33].

$$\Delta G_{PMF} = -RTln\frac{\sum_{ibound} \pi_i}{\sum_{iunbound} \pi_i}$$

Volume correction was used to compare the calculated binding free energy to experiment values.

$$\Delta G_{binding} = \Delta G_{PMF} + \Delta G_V ,$$

Where $\Delta G_V = -RTln(\frac{V_u}{V_0})$, $V_u = 1.142\ nm^3$ is the average system volume of our simulations, and $V_0 = 1.661\ nm^3$ is the standard volume (1M concentration).

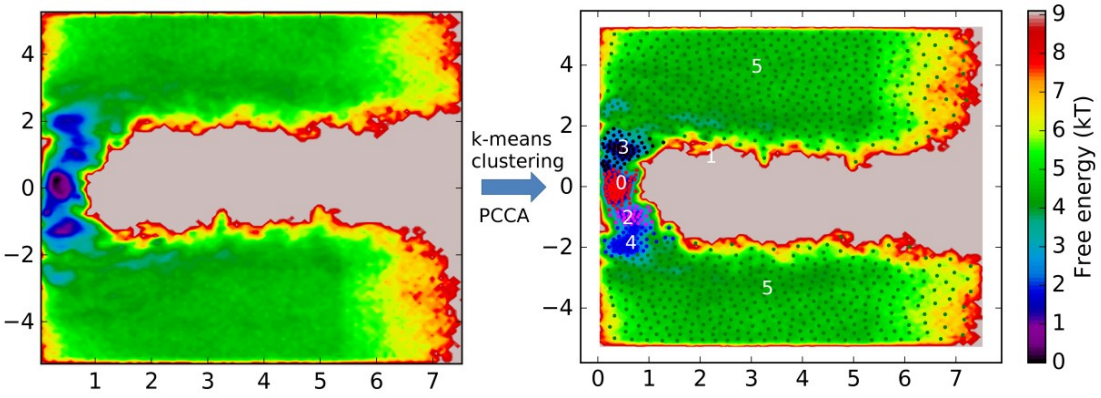

Figure S17. Two dimensional free energy surface of D-glucose transporting on CV2 and CV3 space. 1000 microstates were assigned using k-means clustering method with convergence tolerance of 1e-08. Then the Perron-cluster cluster analysis (PCCA) method was used to compute the microstates into six metastable states.

Table S1. Stationary distribution of six microstates

metastate 0	metastate 1	metastate 2	metastate 3	metastate 4	metastate 5
0.0192513	0.0009621	0.0048578	0.0159373	0.0164480	0.9425433
4	2	5	1	6	2

where $pi_{unboud} = pi_1 + pi_5$

Table S2. Collective variables (CVs) used in this work

CV1	Conformational transition of GLUT1 from its outward-open state to the inward-open state.
CV2	Distance between the center of mass (COM) of the D-glucose and GLUT1 onto the z-axis
CV3	Distance between the center of mass (COM) of the D-glucose and GLUT1 onto the xy-plane

3. GLUT1 Mutants experiments

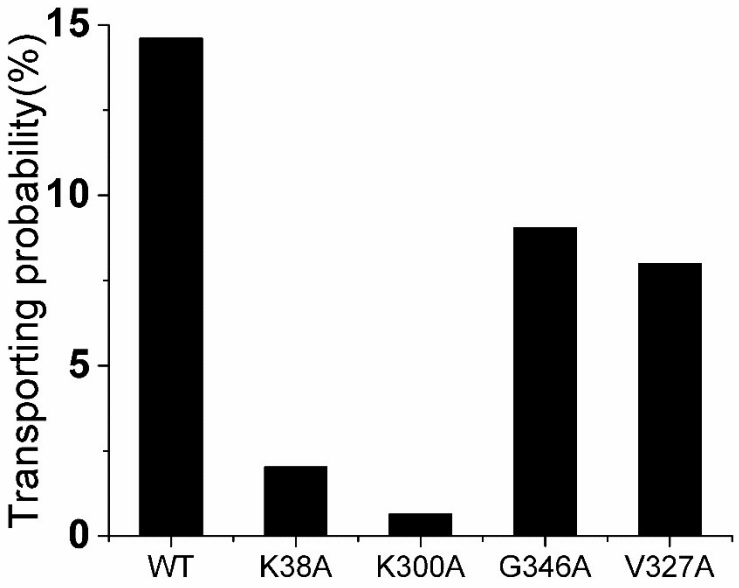

Figure S18. Force tracing measurements performed on wild type of HEK293 cells and cells overexpressed K38A, K300A, G346A and V327A.

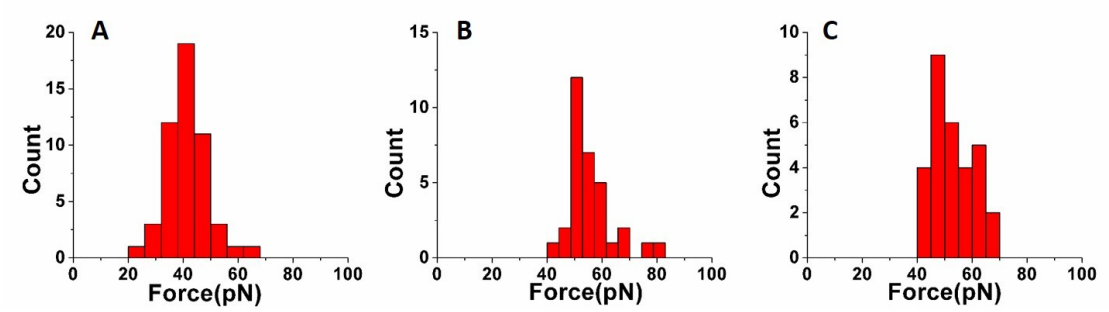

Figure S19. Distribution of the glucose transport force on wild type cells(A), cells overexpressed G346A(B), cells overexpressed V327A(C). The force value is 42± 7pN, 57± 10 pN and 54± 8 pN, respectively.

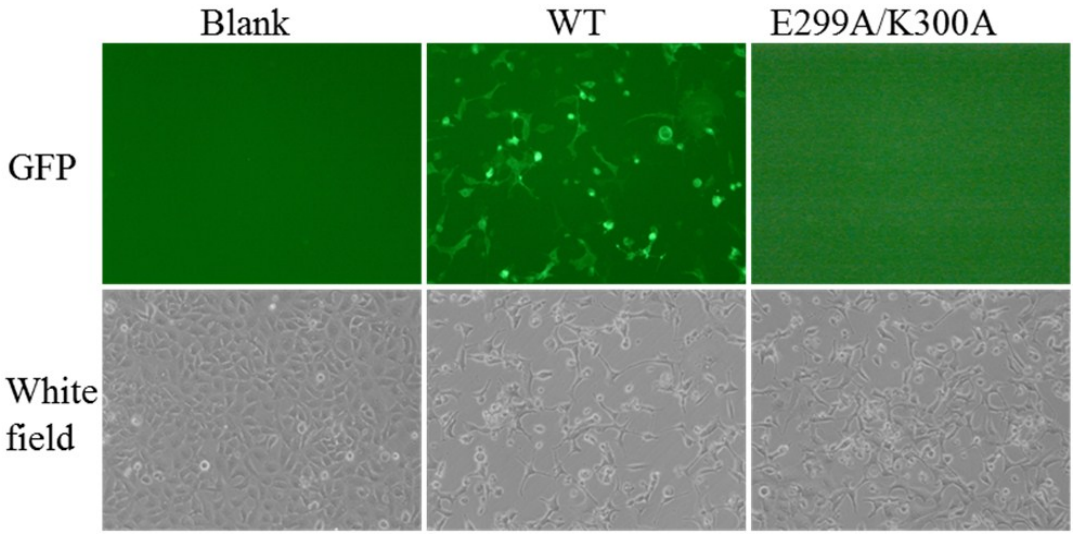

Figure S20.The expression of the double mutant E299A/K300A and WT in HEK293cells.The double mutant (E299A/K300A) has no observed GFP expression in HEK293 cell, implying that mutations of residues E299 and K300 together on TM7 might impair the folding of the mutant.

Methods of experiments:

1. Cell culture:

Parental HeLa and MDCK cells were obtained from ATCC. The cells were cultured on APTES-glass slide in Dulbecco's modified Eagle's medium (DMEM) containing 10% fetal bovine serum, 100 U/ml penicillin, and 100 μg/ml streptomycin at 37 °C with 5% CO_2. The cell line has been tested for mycoplasma contamination.Usually, the cells need to be cultured for 2 or 3 days to achieve 75% confluence on the glass slide. Before performing Force Tracing experiments, the HeLa cells were incubated in a glucose-free

RPMI-1640 medium for 1 hour at 37 °C to remove the extracellular glucose and reduce the intracellular glucose concentration, which caused the cells starved.

2. Modifying glass slide with APTES:

APTES-glass slide substrate was prepared as described[34]. Briefly, a desiccator was purged with argon for 2 minutes, 30 μL APTES (99%) and 10 μL *N*,*N*-diisopropylethylamine (99%) were respectively placed into one small container at bottom of the desiccator; subsequently, the desiccator was purged with argon for another 2 minutes. Glass slides were placed into the prepared desiccator, and then the desiccator was sealed off after purging for further 3 minutes, leaving the glass slides exposedto APTES vapor for 1 hour. After this exposure, the containers with APTES and *N*,*N*-diisopropylethylamine were removed, the desiccator was purged again, and the treated glass slides were stored in the sealed desiccator prior to using.

3. Conjugation of 1-thiol-D-glucose on AFM tips:

Functionalization of AFM tips (Microlever, Veeco, Santa Barbara, CA) with APTES was prepared just as preparing AP-glass slide described above. The cantilevers were cleaned in a UV cleaner, vapor treated with APTES. Subsequently, PEG-crosslinker (MAL-PEG2000-NHS, JenKem Technology Co., Ltd; MAL-PEG690-NHS and MAL-PEG1400-NHS, Biomatrik inc Co., Ltd.) was conjugated in triethylamine and trichloromethane as reference [35]. The tips were then immersed in 1μg/mL 1-thiol-β-D-glucose buffer solution for glucose functionalization. Lastly, the D-glucose tethered AFM tips were rinsed with PBS buffer for three times and stored at 4 ^{o}C until use. The conjugation of antibody of GLUT1 on AFM tip is the same as the conjugation of glucose.

4. Force Tracing measurements:

Force Tracing curve was acquired based on AFM 5500 (Agilent Technologies, Chandler, AZ) in glucose-free RPMI-1640 medium at 37 °C. The shift of the cantilever-deflection signal was collected by a 16 bit DA/AD card (PCI-6361e，National Instruments). The blocking experiments were performed by the addition of D-glucose (final concentration is 6.7 μg/mL) and cytochalasin B (the final concentration is 1

μg/mL) into the culture medium, respectively. The washout experiment was engaged after the blocking experiment of D-glucose, in which the free D-glucose was washed away from the medium and the cells remained starved in glucose-free RPMI-1640 medium again. One thousand tracing curves were recorded at different positions on the cells. The deflection sensitivity of the photo-detector and the spring constant of AFM tip were determined as reference [36]. The data were collected with the low-pass filter of 100Hz or by the 60 point smoothing in Origin7.0 to get rid of high frequency noise from the electronics and environment. The experiments were repeated three times for each condition.

5. Glucose uptake assay:

Site-directed mutagenesis of the human GLUT1 gene was carried out using the QuikChange Lightning Site-Directed Mutagenesis Kit (Agilent, USA). The PCR reaction was performed using 10 ng of Plenti-SLC2A1-mGFP as a template with primers a112g_a113c (5'-gaactcctcgatcaccgcctgggggcattgatg-3'), a1277c 5'-gcttccagtatgtggcgcaactgtgtggtcc-3'), a896c_a898g_a899c (5'-tgctgcacccccgccgccgcgaagatgctcgtgg-3'), a112g_a113c (5'-gaactcctcgatcaccgcctgggggcattgatg-3'), a1277c 5'-gcttccagtatgtggcgcaactgtgtggtcc-3'), a896c_a898g_a899c (5'-tgctgcacccccgccgccgcgaagatgctcgtgg-3'), a112g_a113c(5'-gaactcctcgatcaccgcctgggggcattgatg-3',5'-catcaatgcccccccaggcggtgatcgaggagttc-3'), a898g_a899c (5'-gctgcacccccgccgcctcgaagatgctcg-3',5'-cgagcatcttcgaggcggcgggggtgcagc-3'), a1277c(5'-gcttccagtatgtggcgcaactgtgtggtcc-3',5'-ggaccacacagttgcgccacatactggaagc-3'), a896c_a898g_a899c(5'-tgctgcacccccgccgccgcgaagatgctcgtgg-3',5'-ccacgagcatcttcgcggcggcgggggtgcagca-3'), t980c (5'-ctgctcgctccaccgcaaacagcgacacg-3',5-'cgtgtcgctgtttgcggtggagcgagcag-3), and g1037c (5'-gagtatggcacaagccgccatgccagc-3',5'-gctggcatggcggcttgtgccatactc-3'). After digestion with DpnI, the resulting plasmids containing the mutated GLUT1 gene were transformed into E. coli DH5α competent cells (TIANGEN, USA). The transformed cells were plated on LB chloramphemicol (34 μg/ml) agar plates and incubated at 37°C overnight. Monoclonal colony were selected and shaked culturing in LB liquid culture medium (chloramphemicol 34 μg/ml) at 37℃ overnight. The cells were collected by

centrifugation at 5000 × g for 5 minutes and then subjected to plasmid preparation. The mutants were confirmed by sequencing analyses, and designated as GLUT1-K38A, GLUT1-K300A, GLUT1-E426A GLUT1-E299A/K300A, GLUT1-V327A, andGLUT1-G346 A. HEK293 cell line (ATCC, USA) was cultured in DMEM with 10% FBS. The cell line has been tested for mycoplasma contamination. Cells were seeded into 12-well plate and cultured for overnight. Then the plasmids containing the mutated GLUT1 or WT GLUT1 were transfected into cells using Lipofectamine 3000 Reagent (Invitrogen, L3000015). After 12 hours transfection, the transfection mix was changed with fresh culture medium with 2.3 mg/L D-glucose. Transfected cells were incubated in this medium for another 24 hours. Eventually the medium was collected, and glucose concentration was determined by the glucose oxidase method using Glucose Kit (RONGSHENG). The glucose uptake for each well was normalized by the value of MTS which was performed to measure cell viability.

The data, showing as average±s.e.m., were averaged from 3 replicated experiments. There were 3-well replicates for each experiment. Two-side T-test was applied for comparing the two groups.

6. Determining the GLUT1 number by STORM imaging

The STORM experiment was described previously[37]. In the semi-quantitative analyses, we randomly selected a rectangle area (2*2μm^2) in each cellular membrane to estimate the localization density of per μm^2 via dividing the total number of localizations in per μm^2 by the average number of localizations per single GLUT1 cluster (average 30 localizations per single glut-1 cluster, by analyzing 50 single GLUT1 clusters from three independent experiments). For the density of glut-1 on the cell membrane, we calculated the localization density on cell membrane through diving the total number of localizations in the selected rectangle area by the area size of the rectangle area, then further estimated the density of the glut-1 on cell membrane via diving the localization density by the average number of localizations per single glut-1 cluster.

7. Preparation of lipid membranes

Lipid membranes were prepared with phosphatidylcholine (PC)/phosphatidylglycerol(PG) (7:3 w/w) according to methods as described

previously[38, 39]. Lipids were dissolved in chloroform, dried by N_2, and vacuumed overnight to remove the residue of organic solvents. The lipids were resuspended in 10 mM HEPES and 150 mM NaCl buffer (pH 7.4) by vortex shaking above the phase-transition temperature of phospholipid, then freeze-thaw 5 times and pass about 20 times through two polycarbonate membranes (0.1 μm) with a mini-extruder above the phase-transition temperature of phospholipids until the solution became transparent. The phospholipid concentrations were determined by phosphorus analysis[39, 40].

References:

1. A. E. Pelling, S. Sehati, E. B. Gralla, J. S. Valentine and J. K. Gimzewski, *Science*, 2004, **305**, 1147-1150.
2. Y. Pan, S. Wang, Y. Shan, D. Zhang, J. Gao, M. Zhang, S. Liu, M. Cai, H. Xu, G. Li, Q. Qin and H. Wang, *Small (Weinheim an der Bergstrasse, Germany)*, 2015, **11**, 2782-2788.
3. Y. Pan, F. Zhang, L. Zhang, S. Liu, M. Cai, Y. Shan, X. Wang, H. Wang and H. Wang, *Advanced Science*, 2017, **4**, 1600489.
4. B. A. Kerwin, B. S. Chang, C. V. Gegg, M. Gonnelli, T. Li and G. B. Strambini, *Protein Science : A Publication of the Protein Society*, 2002, **11**, 1825-1833.
5. Q. Huang, I. Yoon, J. Villanueva, K. Kim and D. J. Sirbuly, *Soft Matter*, 2014, **10**, 8001-8010.
6. F. Rico, L. Gonzalez, I. Casuso, M. Puig-Vidal and S. Scheuring, *Science*, 2013, **342**, 741.
7. X. Shang, Y. P. Shan, Y. G. Pan, M. J. Cai, J. G. Jiang and H. D. Wang, *Chem. Commun.*, 2013, **49**, 8163-8165.
8. F. Kienberger, V. P. Pastushenko, G. Kada, H. J. Gruber, C. Riener, H. Schindler and P. Hinterdorfer, *Single Molecules*, 2000, **1**, 123-128.
9. X. Cheng, Y. F. Qi, J. Lee, S. Jo and W. Im, *Biophys J*, 2015, **108**, 159a-159a.
10. E. L. Wu, X. Cheng, S. Jo, H. Rui, K. C. Song, E. M. Davila-Contreras, Y. F. Qi, J. M. Lee, V. Monje-Galvan, R. M. Venable, J. B. Klauda and W. Im, *J Comput Chem*, 2014, **35**, 1997-2004.
11. R. Kumar, V. G. Iyer and W. Im, *Abstr Pap Am Chem S*, 2007, **233**, 273-273.
12. A. D. MacKerell, D. Bashford, M. Bellott, R. L. Dunbrack, J. D. Evanseck, M. J. Field, S. Fischer, J. Gao, H. Guo, S. Ha, D. Joseph-McCarthy, L. Kuchnir, K. Kuczera, F. T. K. Lau, C. Mattos, S. Michnick, T. Ngo, D. T. Nguyen, B. Prodhom, W. E. Reiher, B. Roux, M. Schlenkrich, J. C. Smith, R. Stote, J. Straub, M. Watanabe, J. Wiorkiewicz-Kuczera, D. Yin and M. Karplus, *J Phys Chem B*, 1998, **102**, 3586-3616.
13. J. B. Klauda, R. M. Venable, J. A. Freites, J. W. O'Connor, D. J. Tobias, C. Mondragon-Ramirez, I. Vorobyov, A. D. MacKerell and R. W. Pastor, *J Phys Chem B*, 2010, **114**, 7830-7843.
14. D. Deng, C. Xu, P. Sun, J. Wu, C. Yan, M. Hu and N. Yan, *Nature*, 2014, **510**, 121-125.
15. E. Neria, S. Fischer and M. Karplus, *J Chem Phys*, 1996, **105**, 1902-1921.
16. H. J. C. Berendsen, D. Vanderspoel and R. Vandrunen, *Comput Phys Commun*, 1995, **91**, 43-56.
17. W. G. Hoover, *Phys Rev A*, 1985, **31**, 1695-1697.
18. S. Nose, *J Chem Phys*, 1984, **81**, 511-519.
19. M. Parrinello and A. Rahman, *J Appl Phys*, 1981, **52**, 7182-7190.
20. M. Parrinello and A. Rahman, *Phys Rev Lett*, 1980, **45**, 1196-1199.

21. T. Darden, D. York and L. Pedersen, *J Chem Phys*, 1993, **98**, 10089-10092.
22. B. Hess, H. Bekker, H. J. C. Berendsen and J. G. E. M. Fraaije, *J Comput Chem*, 1997, **18**, 1463-1472.
23. A. Barducci, M. Bonomi, M. K. Prakash and M. Parrinello, *P Natl Acad Sci USA*, 2013, **110**, E4708-E4713.
24. A. Fiser and A. Sali, *Method Enzymol*, 2003, **374**, 461-491.
25. L. Sun, X. Zeng, C. Yan, X. Sun, X. Gong, Y. Rao and N. Yan, *Nature*, 2012, **490**, 361-366.
26. M. Marchi and P. Ballone, *J Chem Phys*, 1999, **110**, 3697-3702.
27. G. A. Tribello, M. Bonomi, D. Branduardi, C. Camilloni and G. Bussi, *Comput Phys Commun*, 2014, **185**, 604-613.
28. A. J. Ilott, S. Palucha, P. Hodgkinson and M. R. Wilson, *J Phys Chem B*, 2013, **117**, 12286-12295.
29. X. H. Huang, G. R. Bowman, S. Bacallado and V. S. Pande, *P Natl Acad Sci USA*, 2009, **106**, 19765-19769.
30. P. Eastman, M. S. Friedrichs, J. D. Chodera, R. J. Radmer, C. M. Bruns, J. P. Ku, K. A. Beauchamp, T. J. Lane, L. P. Wang, D. Shukla, T. Tye, M. Houston, T. Stich, C. Klein, M. R. Shirts and V. S. Pande, *J Chem Theory Comput*, 2013, **9**, 461-469.
31. M. K. Scherer, B. Trendelkamp-Schroer, F. Paul, G. Perez-Hernandez, M. Hoffmann, N. Plattner, C. Wehmeyer, J. H. Prinz and F. Noe, *J Chem Theory Comput*, 2015, **11**, 5525-5542.
32. S. Roblitz and M. Weber, *Adv Data Anal Classi*, 2013, **7**, 147-179.
33. I. Buch, T. Giorgino and G. De Fabritiis, *P Natl Acad Sci USA*, 2011, **108**, 10184-10189.
34. D. Lohr, R. Bash, H. Wang, J. Yodh and S. Lindsay, *Methods (San Diego, Calif.)*, 2007, **41**, 333-341.
35. C. Stroch, *P. Natl. Acad. Sci. USA*, 2004, **101**, 12503-12507.
36. Y. Shan, *Chem. Commun.*, 2011, **47**, 8091-8093.
37. Y. Wang, J. Gao, X. Guo, T. Tong, X. Shi, L. Li, M. Qi, Y. Wang, M. Cai, J. Jiang, C. Xu, H. Ji and H. Wang, *Cell Research*, 2014, **24**, 959-976.
38. Y. Huang, L. He, G. Li, N. Zhai, H. Jiang and Y. Chen, *Protein & Cell*, 2014, **5**, 631-642.
39. S. Sun, G. Zhao, Y. Huang, M. Cai, Y. Shan, H. Wang and Y. Chen, *Sci. Rep.*, 2016, **6**, 29145.
40. N. P. Chongsiriwatana and A. E. Barron, in *Antimicrobial Peptides: Methods and Protocols*, eds. A. Giuliani and A. C. Rinaldi, Humana Press, Totowa, NJ, 2007, DOI: 10.1007/978-1-60761-594-1_12, pp. 171-182.